

Exchange bias in Fe/Ir₂₀Mn₈₀ bilayers: Role of spin-glass like interface and ‘bulk’ antiferromagnet spins

Sagarika Nayak, Palash Kumar Manna, Thiruvengadam Vijayabaskaran, Braj Bhusan Singh and Subhankar Bedanta*

Laboratory for Nanomagnetism and Magnetic Materials (LNMM), School of Physical Sciences, National Institute of Science Education and Research (NISER), HBNI, P.O.- Bhipur Padanpur, Via –Jatni, 752050, India

Email: Subhankar Bedanta - sbedanta@niser.ac.in

* Corresponding author

Abstract

We have performed magnetic measurements like temperature (T), cooling field (H_{FC}) dependence of exchange bias (EB) and training effect to investigate the magnetic nature of the interface of the Fe/Ir₂₀Mn₈₀ systems. Thin film bilayer samples of different thicknesses of Ir₂₀Mn₈₀ have been prepared by dc magnetron sputtering at room temperature. The variation of exchange bias field (H_{EB}) with the increase in thickness of Ir₂₀Mn₈₀ predicts the antiferromagnet (AFM) ‘bulk’ spins contribution to EB. Exponential decay of H_{EB} and coercive field (H_C) with temperature reveals the presence of spin glass (SG) like interface. Also, the decrease of H_{EB} with increasing H_{FC} confirms the SG like frustration at the interface. Further, the fitting of training effect experimental data envisages the presence of frozen and rotatable spins at the magnetically frustrated interface of these EB systems.

Keywords

Spin glass like interface; frozen and rotatable spins; ‘bulk’ AFM spins; exchange bias; exponential decay

Introduction

The exchange coupling at the interface of ferromagnet (FM)/AFM system [1] develops a unidirectional anisotropy [2-4] in the FM layer, which leads to horizontal shift [5,6] and broadening in the hysteresis loop [7]. Although, EB as an interfacial interaction between FM and AFM is widely studied [8] but the ‘bulk’ spin contribution to EB is still not fully established [9]. However, EB effects have been widely explored for the fundamental understanding and for its technological applications in constructing spintronic based devices such as spin valves, and magnetic random-access memories (MRAMs) etc [6,9-12].

The presence of interfacial spins and their behaviour play critical role for the origin of EB and the training effect where EB decreases with number of cycles of hysteresis loop measurement. It is reported in literature that the interface of the FM and AFM phase can be spin glass (SG) like disorder [12], compensated AFM order or uncompensated FM order. The structural disorder [12], interface roughness [13], chemical intermixing [13], interdiffusion [13] and lack of structural periodicity [12] might be a reason for this glassy state at the interface. The interface is assumed to play a key role in EB, however the AFM ‘bulk’ can also sometimes play an important role [10]. The H_{EB} depends primarily on the defects present at the FM/AFM interface but rather on the presence of the defects in the ‘bulk’ part of the AFM [14]. Further, it is found from a number of experimental evidences that the H_{EB} depends on the AFM layer thickness [15-17] which exists even for higher thicknesses of AFM confirms the contribution of spins from ‘bulk’ part of the AFM to the EB [18-22]. It is found by the various reports that EB still exists by inserting a non-magnetic layer in between FM and AFM layer [10]. Therefore, the understating the role of the various types of interfacial spins and the ‘bulk’ AFM spins may lead to unveil the origin of the EB.

In the present study we report the magnetic nature of the interface from various magnetic measurements. In order to probe the role of ‘bulk’ spins we varied the thickness of $\text{Ir}_{20}\text{Mn}_{80}$ layer for the fixed Fe layer thickness. The trend of H_{EB} and H_C with temperature and H_{FC} indicates the presence of SG like interface in the FM/AFM system. From the fitting of the training effect experimental data, we found that both the frozen and rotatable interfacial frustrated spins contribute to the EB. The rotatable interfacial spins are found to be relax 8 times faster than the frozen interfacial spins.

Table 1: the sample nomenclature and structure for all the samples.

Sample name	Sample structure
S1	Si (100)/Ta (1 nm)/Cu (10 nm)/IrMn (10 nm)/Fe (10 nm)/Cu (3 nm)
S2	Si (100)/Ta (1 nm)/Cu (10 nm)/IrMn (5 nm)/Fe (10 nm)/Cu (3 nm)
S3	Si (100)/Ta (1 nm)/Cu (10 nm)/IrMn (3 nm)/Fe (10 nm)/Cu (3 nm)

Experimental Details

We have deposited Fe/Ir₂₀Mn₈₀ bilayers on Si (100) substrate having native oxide layer by dc magnetron sputtering at room temperature. Sample nomenclature and structure of all the samples are given in table I. Cu of 10 nm thickness has been deposited on top of Ta of 1 nm thickness as seed layer. To avoid oxidation, Cu of 3 nm thickness has been deposited as capping layer. All the thin film layers have been fabricated in a high vacuum chamber manufactured by Mantis deposition Ltd., UK. The base pressure was better than 3×10^{-8} mbar and the Ar working pressure was 5×10^{-8} mbar. The magnetic measurements such as training effect, H_{FC} and temperature dependence of EB were performed using magnetic property measuring system (MPMS 3) manufactured by Quantum design. Grazing incidence x-ray diffraction (GIXRD) measurement was done with x-ray diffractometer from Rigaku equipped with Cu-K α x-ray source.

Results and Discussion

Samples S1-S3 have diffraction peaks correspond to both Fe and IrMn layers at diffraction angle 2θ of 41.9° , 43.2° and 43.5° found in the GIXRD data for all the bilayer thin films (Figure S1 in supplementary material). Fe (111) peak with cubic face-centred crystal structure is found for all the samples. Along with Fe (111) peak, all the samples have IrMn (111) peak with tetragonal primitive crystal structure.

Figure 1 (a) and (b) depict the trend of H_{EB} and H_C vs T of the samples S1-S3. The values of H_{EB} and H_C are taken from the hysteresis loops measured at each temperature after cooling from 400 K in the presence of 1 Tesla (T) magnetic

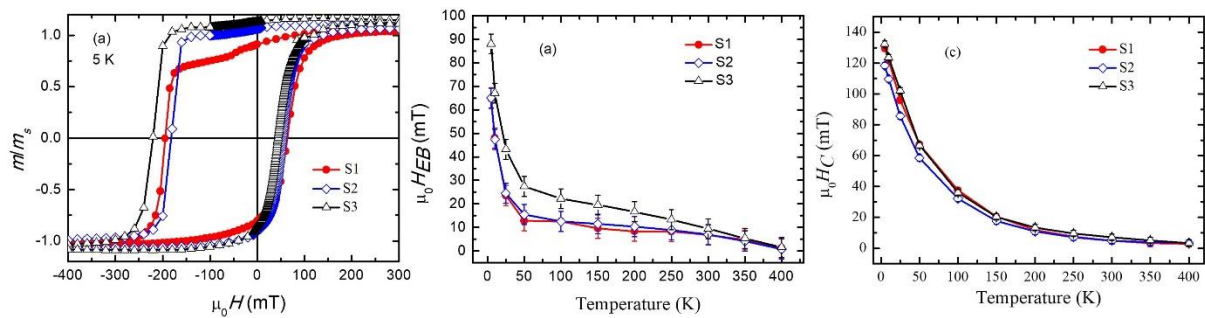


Figure 1: shows the hysteresis loops (a) variation of H_{EB} (a) and H_C (b) vs temperature (T) for all the samples.

field. It has been found from literatures that in the conventional FM/AFM system the maximum value in HEB occurs at minimum value in H_C in a temperature dependent measurement [8]. However, in a system with SG like interface the values of H_{EB} and H_C are found to follow a similar trend [fig. 1(b) and (c)]. We

observed exponential decay of H_{EB} and H_C with increasing temperature in all the samples. The exponential decay of the H_{EB} with increasing temperature is due to the increase in long range AFM ordering and hence the increase in the exchange anisotropy [23]. But we observed both the H_{EB} and H_C are decreasing with increasing temperature. This type of decay for both the H_{EB} and H_C has been generally observed in magnetically frustrated system. As in this study the blocking temperature is too high, the interfacial frustrated disorder state might be a reason behind this decay behaviour in the H_{EB} , H_C vs T plots [24]. If the interface of the FM/AFM system is not frustrated then we may not observe this type of decay of H_{EB} and H_C with temperature. The blocking temperature at which the EB vanishes is found to be ~ 400 K for all the samples. At temperatures above 50 K the H_{EB} gradually decreases with temperature due to thermal excitations [7]. Also, the interfacial spins become uncorrelated due to thermal energy [12]. Therefore, at higher temperatures the interfacial AFM spins under the polarizing action of the ‘bulk’ AFM contribute to the H_{EB} and low anisotropy interfacial spins contribute to the H_C . We have found a sudden rise of H_{EB} and H_C at lower temperatures below 50 K possibly due to freezing of spin glass like interfacial spins [7]. Our observations are corroborated with findings of the Fulara *et al.* [7] in the Fe/Ir₂₀Mn₈₀ layer structures. Thus, this temperature dependent study elucidates the presence of SG like interface in these EB systems.

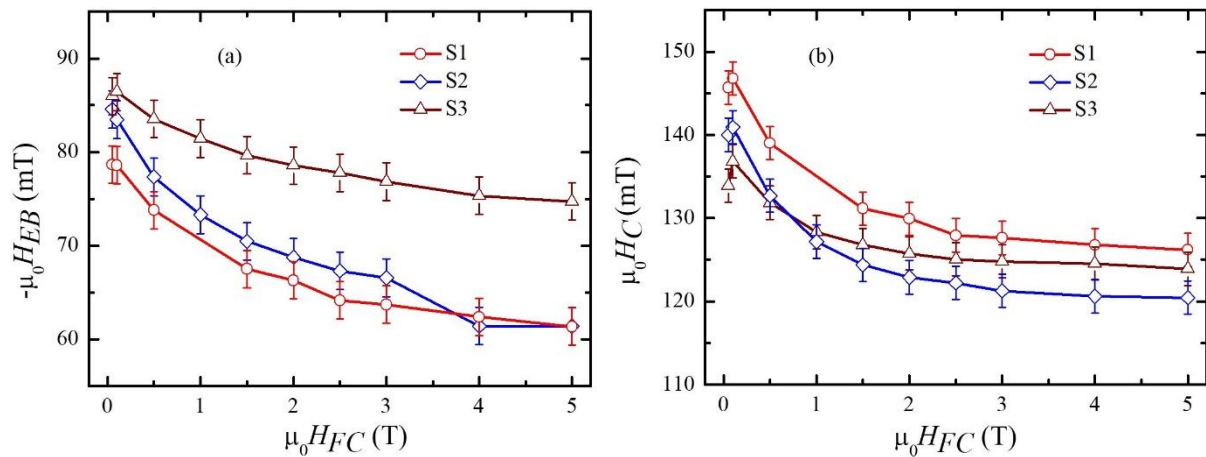


Figure 2: shows the cooling field (H_{FC}) dependence of (a) H_{EB} , (b) H_C for samples S1-S3.

Figure 2 (a) and (b) show the variation of H_{EB} and H_C with H_{FC} for samples S1-S3. We have cooled our bilayer samples from 400 K to 5 K in presence of different magnetic fields (500 Oe to 5 T). In conventional FM/AFM system, the H_{EB} increases with increasing H_{FC} [25]. More numbers of spins are getting pinned in the H_{FC} direction and that increases with increase in the H_{FC} . Again, the cooling field acts on the ‘bulk’ of the AFM to induce magnetization in the AFM [14]. However, in the FM/SG system the H_{EB} decreases with increasing HFC [26] due to random interface effect [14]. The cooling field acts on the ‘bulk’ of the SG to induce some magnetization [14]. But, the random interaction in the ‘bulk’ and interface of FM/SG systems gives rise to the cancellation of the magnetization

[14]. In our Fe/Ir₂₀Mn₈₀ system, we observed monotonous decrease of H_{EB} and H_C with H_{FC} . The spin glass like interaction at the interface of Fe and Ir₂₀Mn₈₀ might be a reason for this type of behaviour of H_{EB} and H_C with H_{FC} .

Figure 3 shows the AFM thickness dependence of EB at different cooling fields. In this study, we found that the H_{EB} is decreasing with increasing the thickness of AFM layer from 3 to 5 nm after this it levels off. In literature, it is found that there is a critical thickness of AFM layer where the onset of EB occurs [8]. It is reported that in sputter deposited thin film samples the critical thickness is above ~ 5 nm [27]. the critical thickness, H_{EB} continues to increase and then a peak in H_{EB} is found [8]. After the peak a decrease in H_{EB} is found followed by

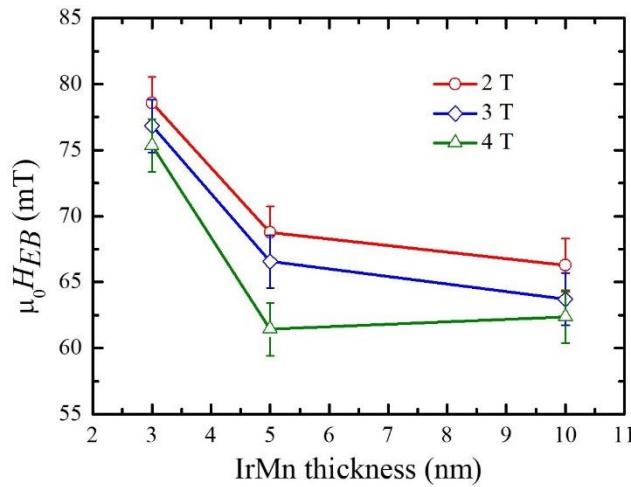


Figure 3: shows the IrMn thickness dependence of exchange bias for cooling field of 2, 3 and 4 T.

saturation [8]. However, in our bilayer samples the AFM thickness is more than the critical thickness. Similar results were found in literature with the explanation of formation of partial domain wall in the AFM parallel to the interface [8]. The reason for this type of AFM thickness dependence may be due to the microstructural changes of the AFM layer as one kind of orientation is not stable above some thickness [28]. The AFM thickness dependence behaviour has also been explained theoretically that there may be the change in AFM domain structure with the thickness of AFM and therefore the variation of H_{EB} with thickness of AFM has been observed [28,29]. Thus, the thickness dependence study gives an overview of the contribution of volume part of the AFM to the EB.

Fig 4 (a)-(c) show the M-H loops taken after field cooling the system at 1 T field from 400 K to 5 K for samples S1-S3. The circle (1st), triangle (2nd) and square (10th) symbols hysteresis loops are shown in the figure 4. 4 (d)-(f) show the H_{EB} plotted as a function of loop number n (training effect).

In order to understand the relaxation behaviour of the interface spins, first we fitted the H_{EB} vs n data with the following empirical power law formula [30];

$$H_{EB}(n)=H_{EB\infty}+K/\sqrt{n} \quad \dots\dots\dots (1)$$

Where, $H_{EB}(n)$ is the exchange bias field for the n th loop run, $H_{EB\infty}$ is the exchange bias field after infinite number of loops run, K is the system dependent constant. We found that the power law given in eq. (1) can fit well the

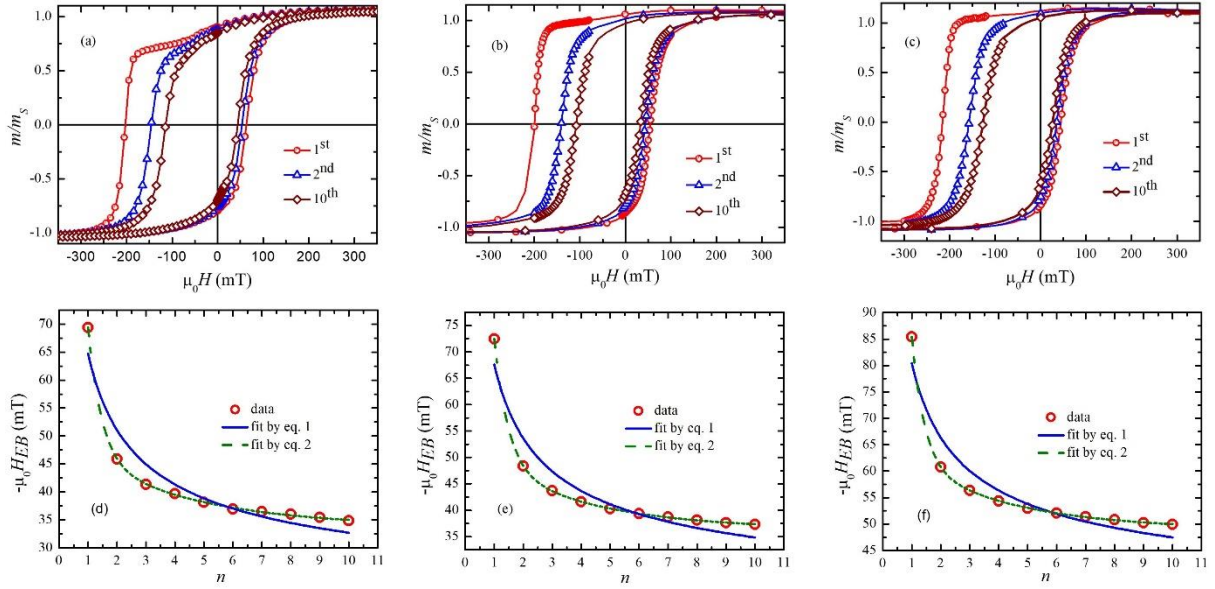


Figure 4: 1st, 2nd and 10th subsequent hysteresis loops of (a) S1, (b) S2 and (c) S3; variation of H_{EB} vs n for (d) S1, (e) S2 and (f) S3. In figures (d), (e) and (f), the open circles are experimental data, solid and segment lines are the fitted data.

experimental data for $n > 1$ only and cannot fit the steep relaxation data between $n=1$ and 2. The $H_{EB\infty}$ and K values show a systematic increase with decreasing the $\text{Ir}_{20}\text{Mn}_{80}$ layer thickness. Next, we considered a SG approach [11] containing both the frozen and rotatable interfacial spins of the FM/AFM system. We fitted the H_{EB} vs n data for all the samples by the double exponential decay function [11] which is specific for SG like frustrated interface:

$$H_{EB}(n)= H_{EB\infty}+A_f \exp (-n/P_f)+A_i \exp (-n/P_i) \quad \dots\dots\dots (2)$$

Where, A_f , P_f are the parameters for the interfacial frozen spins and A_i , P_i are the parameters for the interfacial rotatable spins of the FM and AFM interface. A_f , A_i have the dimension of mT and P_f , P_i are dimensionless. P_f and P_i are the relaxation rates of the frozen and rotatable interfacial spin components, respectively. From the R^2 value, we can estimate the excellent fit of the training effect experimental data. The parameters obtained after fitting the training effect data with eq. (1) and (2) are given in table II. It is found the the fitting parameter $H_{EB\infty}$ shows a systematic decrease from 48.9 mT to 33.8 mT with increasing the thickness of

Ir₂₀Mn₈₀ from 3 to 10 nm. The weighing factors A_i shows a systematic decrease with increasing Ir₂₀Mn₈₀ film thickness. However, the weighing factor A_f value shows a little discrepancy in sample S2. The weighing factor A_f is always higher than the A_i indicating that the training effect is mainly due to the frozen spin component [6]. But we found that the relaxation rates of the frozen and rotatable interfacial spin components P_f and P_i remain constant for all the three samples. We calculated that the ratio P_i/P_f for all the samples remains at 8. Thus, the relaxation rate of the interfacial rotatable spin component is almost 8 times faster than the interfacial frozen spin component. We can conclude that by considering both the interfacial frozen and rotatable spin components one can fit the experimental training effect data satisfactorily.

Table 2: fitting parameters obtained from the H_{EB} vs n plot for all the samples by fitting eq. (1) and (2).

Sample	Equation (1) parameters		Equation (2) parameters					
	$H_{EB\infty}$ (mT)	K (mT)	$H_{EB\infty}$ (mT)	A_f (mT)	P_f	A_i (mT)	P_i	P_i/P_f
S1	17.9 ± 2.6	46.8 ± 4.8	33.8 ± 0.6	206.4 ± 34.3	0.46 ± 0.04	15.8 ± 1.6	3.93 ± 0.7	8.54
S2	19.7 ± 2.7	47.9 ± 5.0	36.4 ± 0.2	199.5 ± 11.5	0.47 ± 0.02	16.0 ± 0.8	3.56 ± 0.2	7.57
S3	32.3 ± 2.8	48.1 ± 5.2	48.9 ± 0.2	243.5 ± 16.6	0.43 ± 0.02	16.5 ± 0.7	3.58 ± 0.2	8.33

In the FM/AFM system the relaxation can be due to thermal or athermal effects [6]. The thermal training effects results into the gradual decrease of H_{EB} with number of loops n . Due to the thermal activation, the AFM uncompensated spins are reconfigured from the original configuration [6]. In athermal training effect, there is a large reduction in H_{EB} and H_C between the first and second subsequent hysteresis loops afterwards a gradual decrease in H_{EB} and H_C is found. This type of relaxation arises due to the metastable state of the AFM spins [6]. We can conclude that the interfacial SG like structure frozen into a metastable stable state during FC and that metastable state relaxes resulting into the large reduction in the H_{EB} and H_C values in the second subsequent loop [6].

Thus, this study develops our general understanding in the role of interfacial SG state on the magnetic properties. Again, the training effect data tells that both the frozen and rotatable spins have effect in EB. Also, we investigated the relaxation rate of rotatable spins wrt the frozen spins.

In conclusion, we investigated the temperature, H_{FC} dependence of EB and training effect in sputter-deposited Fe/Ir₂₀Mn₈₀ systems. We observed exponential decay behaviour in H_{EB} , H_C with temperature. We found decrease in H_{EB} with increase in H_{FC} contrary to the typical behaviour H_{EB} with H_{FC} in FM/AFM systems. It is found that the SG like interface might be a primary reason for this type of trend in H_{FC} and temperature dependence of EB. However, the contribution of ‘bulk’ part of the AFM spins to EB from the variation of H_{EB} with the thickness of AFM is also observed. Training effect has been analysed by fitting a model which consider both frozen and rotatable spins. We found that the interfacial rotatable spins relax 8 times faster than the interfacial frozen spins.

Supporting Information

Supporting information file 1: the GIXRD (Figure S1) data of all the samples.

File Name: S1.pdf

Format: pdf

Acknowledgements

The authors thank Department of Atomic Energy (DAE) and Department of Science and Technology-Science and Engineering Research Board (SB/S2/CMP-107/2013), Government of India for providing the financial support.

References

1. Nogues, J.; Sort, J.; Langlais, V.; Skumryev, V.; Surinach, S.; Manoz, J. S.; Baro, M. D.; *Phys. Reports* **2005**, 458, 422.
2. Stamps, R. L. *J. Phys. D: Appl. Phys.* **2008**, 33, R247.
3. Berkowitz, A. E.; Takano, K. *J. Magn. Magn. Mater.* **1999**, 200, 552.
4. Kiwi, M. *J. Magn. Magn. Mater.* **2001**, 234, 584.
5. Ohldag, H.; Scholl, A.; Nolting, F.; 182 Arenholz, E.; Maat, S.; Young, A. T.; Carey, M.; Stohr, J. *Phys. Rev. Lett.* **2003**, 91, 1.
6. Muhammed Shameem, P.V.; Senthil Kumar, M. *J. Magn. Magn. Mater.* **2018**, 458, 241-252.
7. Fulara, F.; Chaudhary, S.; Kashyap, S. C.; Granvill, S. *J. Appl. Phys.* **2014**, 115, 043910.
8. Ali, M.; Marrows, C. H.; Al-Jawad, M.; Hickey, B. J.; Misra, A.; Nowak, U.; Usadel, K. *D. Phys. Rev. B* **2003**, 68, 214420.
9. Basaran, Ali C.; Saerbeck, T.; Venta, J. de la; Huckfeldt, H.; Ehresmann, A.; Schuller, Ivan K. *Appl. Phys. Lett.* **2014**, 105, 072403.
10. Nam, D. N. H.; Chen, W.; West, K. G.; Kirkwood, D. M.; Lu, J.; Wolf, S. A.; *Appl. Phys. Lett.* **2008**, 93, 152504.
11. Mishra, S. K.; Radu, F.; Durr H. A.; Eberhardt, W. *Phys. Rev. Lett.* **2009**, 102, 177208.
12. Spizzo, F.; Tamisari, M.; Chinni, F.; Bonfiglioli, E.; Del Bianco, L. *J. Magn. Magn. Mater.* **2017**, 421, 234-240.
13. Radu, Florin *Dissertation* **2005**
14. Usadel, K. D.; Nowak, U. *Phys. Rev. B* **2009**, 80, 014418.
15. Lai, Chih-Huang; Matsuyama, Hideo; White, Robert L.; Anthony, Thomas C.; Bush, Gary G. *J. Appl. Phys.* **1996**, 79, 6389.
16. McCord, Jeffrey; Hamann, Christine; Schafer, Rudolf; Schultz, Ludwig; Mattheis, Roland *Phys. Rev. B* **2008**, 78, 094419.
17. McCord, J.; Mangin, S. *Phys. Rev. B* **2013**, 88, 014416.
18. Ambrose, T.; Chien, C. L. *J. Appl. Phys.* **1998**, 83, 6822.
19. Milteny, 204 P.; Gierlings, M.; Keller, J.; Beschoten, B.; Guntherodt, G.; Nowak, U.; Usadel, K. *D. Phys. Rev. Lett.* **2000**, 84, 4224.
20. Malinowski, G.; Hehn, M.; Robert, S.; Lenoble, O.; Schuhl, A.; Panissod, P. *Phys. Rev. B* **2003**, 68, 184404.
21. Dutson, J. D.; Huerrich, C.; Vallejo-Fernandez, G.; Fernandez-Outon, L. E.; Yi, G.; Mao, S.; Chantrell, R. W.; O'Grady, K. *J. Phys. D: Appl. Phys.* **2007**, 40, 1293.

22. Morales, R.; Li, Z. P.; Olamit, J.; Liu, K.; Alameda, J. M.; Schuller, I. K. *Phys. Rev. Lett.* **2009**, *102*, 097201.
23. Barman, J.; Bora, T.; Ravi, S. *J. Magn. Magn. Mater.* **2015**, *385*, 93.
24. Wang, C.; Zhou, L.; Fu, Q.; Tian, Y.; Wanga, S.; Gou, H.; Ai, J.; Zhang, L.; Xue, F.; *J. Magn. Magn. Mater.* **2018**, *449*, 372-377.
25. Bianco, L. D.; Spizzo, F.; Tamisari, M.; Laureti, S. *Solid State Commun.* **2011**, *151*, 351-353.
26. Rui, W. B.; Hu, Y.; Du, A.; You, B.; Xiao, M. W.; Zhang, W.; Zhou, S. M.; Du, J. *Sci. Rep.* **2015**, *5*, 13640.
27. Svalov, A. V.; Kurlyandskaya, G. V.; Lepalovskij, V. N.; Savin, P. A.; Vas'kovskiy, V. O. *Superlattices and Microstructures* **2015**, *83*, 216.
28. Nogues, J.; Schuller, Ivan K. *J. Magn. Magn. Mater.* **1999**, *192*, 203-232.
29. Malozemoff, A.P. *Phys. Rev. B* **1988**, *37*, 7673.
30. Paccard, D.; Schlenker, C.; Massenet, O.; Montmory, R.; Yelon, A. *Phys. Status Solidi* **1966**, *16*, 301.